Effects of rapid thermal annealing on the room-temperature NO_2-sensing properties of WO_3 thin films under LED radiation*

Hu Ming(胡 明)†, Jia Ding-Li(贾丁立), Liu Qing-Lin(刘青林), Li Ming-Da(李明达), and Sun Peng(孙 鹏)

School of Electronics and Information Engineering, Tianjin University, Tianjin 300072, *China*

(Received 14 November 2012; revised manuscript received 12 January 2013)

WO_3 thin films were sputtered onto alumina substrates by DC facing-target magnetron sputtering. One sample was rapid-thermal-annealed (RTA) at 600 °C in a gas mixture of N_2:O_2 = 4 : 1, and as a comparison, another was conventionally thermal-annealed at 600 °C in air. The morphology of both was investigated by scanning electron microscopy (SEM) and atomic force microscopy (AFM), and the crystallization structure and phase identification were characterized by X-ray diffraction (XRD). The NO_2-sensing measurements were taken under LED light at room temperature. The sensitivity of the RTA-treated sample was found to be high, up to nearly 100, whereas the sensitivity of the conventionally thermal-annealed sample was about five under the same conditions. From the much better selectivity and response-recovery characteristics, it can be concluded that compared to conventional thermal annealing, RTA has a greater effect on the NO_2-sensing properties of WO_3 thin films.

Keywords: gas sensor, tungsten-oxide thin film, rapid thermal annealing, LED

PACS: 82.47.Rs, 73.61.Cw, 81.40.Ef, 85.60.Jb **DOI:** 10.1088/1674-1056/22/6/068204

1. Introduction

With the development of modern industry, environmental problems are an increasing threat to human health and safety. A large proportion of air-polluting gases are nitrogen oxides such as NO_2. Environmental monitoring and protection are widespread concerns worldwide.[1] In many fields, such as environmental stewardship, energy management, car design, food safety, and medical care, demands are increasing for various types of high-performance gas sensors. Therefore, the study of various types of gas detection with rapidly reversing response, which can detect low concentrations of gas, especially nitrogen oxide, has become increasingly prominent.

Semiconducting metal oxides such as TiO_2, ZnO, SnO_2, InO_2, WO_3, Cr_2O_3, Nb_2O_5, and MoO_3[2–7] can be utilized as solid-state gas-sensing materials and have been widely used for air pollution detection, by taking advantage of their resistance changes in the presence of particular gases. For example, Cr_2O_3 hollow nanospheres (HNs) were synthesized via a hydrothermal approach. The room-temperature (RT) gas sensing properties of Cr_2O_3 HNs reach below 5 ppm.[8] In/Pd-doped SnO_2 was synthesized via a sol–gel method and coated on a silicon substrate with Pt electrodes to fabricate a microstructure sensor.[9]

In recent years, some composite materials have been synthesized to detect many kinds of gas. For example, excellent CH_4 sensing properties are found in In–Pd–Co–SnO_2 composite nanofiber micro-sensors, which have been synthesized using an electrospinning method.[10] Humidity sensors with double-layer sensing films of ZnO and TiO_2 nanofibers have been synthesized via electrospinning methods, and excellent stability, rapid response and recovery times were found.[11,12] An interesting composite, a KCl/mobil composition of matter-41 (MCM-41), has been synthesized via a heat-treating process, and exhibits improved humidity sensing properties.[13]

Among these semiconducting metal oxides, WO_3 is considered to be one of the most attractive materials for making semiconducting metal–oxide gas sensors.

Due to the slow and appreciable interaction of the surrounding gas with the surface of the sensing layer at room temperature (RT), the working temperature of the WO_3 thin-film gas sensor reaches high levels, up to about 250 °C,[14] and a heating element is required, increasing power consumption and hindering integration with the silicon substrate. Moreover, the high temperature could even trigger an explosion in some conditions. Therefore, there is an essential need for the development of gas sensors that can be operated at lower temperatures (even at RT) with enhanced response.

In order to solve this problem, in recent years some researchers[15,16] have used ultraviolet (UV) radiation to reduce the working temperature of the metal–oxide gas sensors. Because the UV light source is inconvenient and hampers integration of the IC, some researchers[17] have used visible light (including LEDs) to reduce the working temperature of metal–oxide gas sensors. But problems such as low sensitivity, slow response, and slow recovery still exist.

*Project supported by the National Natural Science Foundation of China (Grant Nos. 62171070, 60771019, and 60801018) and Tianjin Key Research Program of Application Foundation and Advanced Technology, China (Grant No. 11JCZDJC15300).

†Corresponding author. E-mail: huming@tju.edu.cn

© 2013 Chinese Physical Society and IOP Publishing Ltd

In order to get a room-temperature thin-film gas sensor with high sensitivity, fast response, and fast recovery, nanomaterials with higher surface interaction rates, narrow band gaps and light-activated properties are needed. Conventional metal–oxide semiconductors such as ZnO and SnO_2 are unsuitable for activation by visible light (including LEDs).[17] WO_3,[18] an important n-type semiconductor with a narrow band gap ($\sim$ 2.56 eV), is widely used to detect various gases.[19–24] In the experiment described herein, we found that rapid thermal annealing can give WO_3 much better room-temperature gas-sensing properties under LED irradiation. However, there have been no reports about the effects of rapid thermal annealing on LED light-activated WO_3 room-temperature thin-film gas sensors. This paper reports the fabrication method and experimental testing of WO_3 thin-film gas sensors on alumina substrates that work at RT.

2. Experiment

Alumina substrates measuring 10 mm$\times$25 mm were ultrasonically cleaned with deionized water, acetone, and ethanol successively, for 10 minutes in each step, to remove grease and other impurities from the surface, and then dried naturally.

The DPS-III ultra-high vacuum facing-target magnetron sputtering system was used to deposit the films. With the help of an interdigitated shadow mask, a pair of interdigitated Pt electrodes was deposited on the cleaned alumina substrate, using RF magnetron sputtering and a circular Pt target 60 mm in diameter with a purity of 99.95% (supplied by GRIKIN Advanced Materials Co). The thickness of the Pt electrodes is about 100 nm, and the distance between the two contact points of the Pt electrodes is about 5 mm.

A DC facing-target magnetron sputtering method was then used for depositing the WO_3 thin film, using a circular tungsten target of 60 mm in diameter with a purity of 99.95% (manufactured by GRIKIN Advanced Materials Co). The WO_3 thin film is 20 mm$\times$10 mm, with the contact points of the Pt electrodes uncovered, as can be seen from Fig. 1. The thickness of the WO_3 thin film is about 200 nm, as measured by an XP-2 profiler.

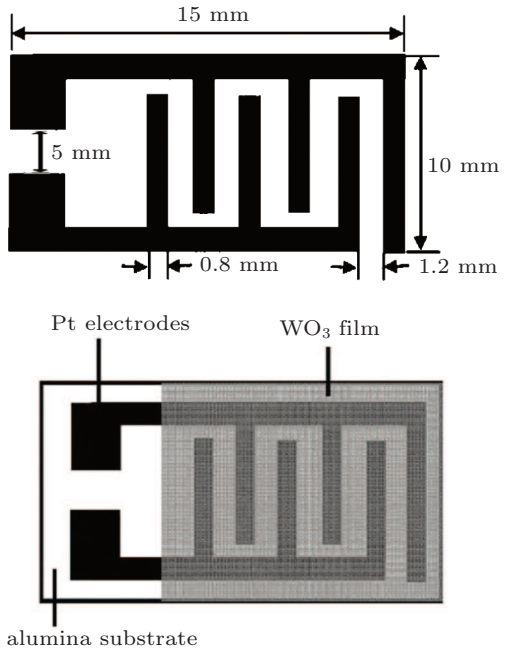


Fig. 1. Schematic diagram of the WO_3 thin-film gas sensor.

The sputtering conditions for the Pt electrodes and WO_3 films are shown in Table 1.

Then the as-deposited WO_3 film was annealed by the rapid annealing furnace (AG610, manufactured by Allwin21 Corp., USA) and marked as sample 1 (S1). For comparison, sample 2 (S2) was obtained by annealing the as-deposited WO_3 thin film at 600 °C[14] with a muffle furnace. The annealing conditions of conventional thermal annealing[25] and RTA (rapid thermal annealing) can be seen in Table 2.

Table 1. The sputtering conditions for the Pt and WO_3 thin films.

Deposited	Target composition	Base pressure/Pa	Sputtering pressure/Pa	Sputtering gas	Sputtering power/W	Sputtering time/min	Substrate temperature
Pt	Pt (99.95%)	$4.0\text{x}10^{-4}$	2.0	pure Ar	100	10	RT
WO_3	W (99.95%)	4.0×10^{-4}	1.0	Ar:O_2 = 9:1	100	60	RT

Table 2. The annealing conditions for the WO_3 thin films.

Sample	Annealing temperature/°C	Annealing equipment	Ramping rate	Annealing gas	Holding time	Cooling time
S1(RTA)	600	rapid annealing furnace	20 °C/s	N_2:O_2 = 4:1	90 s	120 s
S2	600	muffle furnace	2 °C/min	air	4 h	8 h

The surface morphology and crystal structure of the WO_3 films were measured by a field emission scanning electron microscope (FESEM, FEI Nanosem 430, and Hitachi S-4800), an atomic force microscope (AFM, Nanosurf easyScan2) and an X-ray diffractometer (XRD, RIGAKU D/MAX 2500 V/PC, Cu K_α radiation).

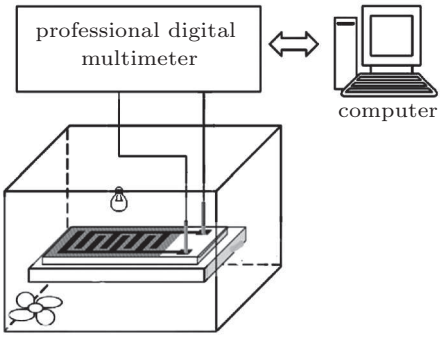


Fig. 2. Schematic diagram of the gas sensing test system.

The gas sensing characteristics were measured in a static gas-sensing testing system consisting of a polymethyl methacrylate (PMMA) test chamber, a 0.7-W LED lamp (λ = 397 nm), a digital multimeter (UT70D) and an automatic data acquisition system.[26] The gas sensing measurements were made at RT with a relative humidity of 40% (controlled by a dehumidifier, DH25EA GREE) and in darkness. The light intensity was 100 lx, which was measured by a portable optometer (model S471, made by UDT instruments). A schematic diagram of the gas sensing test system is shown in Fig. 2. The resistance data was obtained by the digital multimeter and then sent to a PC for further analysis.

The sensor response (S) to NO_2 is defined as $S = (R_{gas} - R_{air})/R_{air}$, where R_{gas} and R_{air} denote the resistance of the sensor under exposure to the measuring gas and in clear air, respectively. The response time is defined as the time when 90% of the responsive resistance change is completed, omitting the recovery time.

Finally, the LED lamp was switched off, and the change in resistance after darkening was also recorded.

3. Results and discussion

3.1. Microstructure characterizations

In order to investigate the morphological difference between S1 and S2, surface SEM images were taken. Figure 3 shows SEM images of the surface of the WO_3 film before annealing, and two annealed samples. It can be seen that the thermal annealing[25] results in clear grain boundaries of varying sizes that indicate the WO_3 thin films were crystallized (Figs. 3(b)–3(c)). It can also be seen that, compared with S2, S1 seems to have a looser structure because of the much more rapid thermal change, and cracks have appeared on the surface. The size of the S1 particles are much smaller, exhibiting a larger combined surface area than those of S2. The compact flat surface of the WO_3 thin film before annealing can be seen in Fig. 3(a).

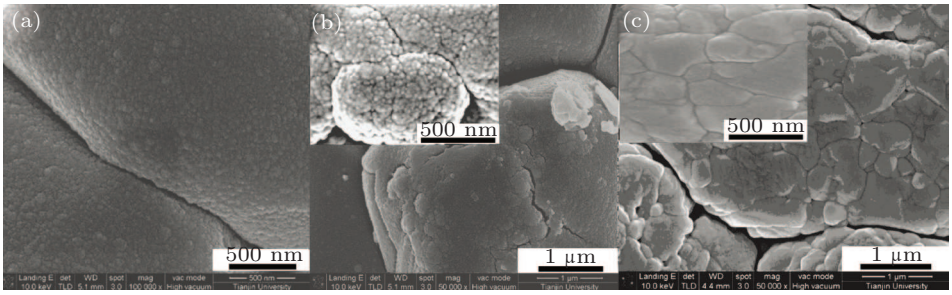


Fig. 3. SEM images of the WO_3 thin film: (a) before annealing, (b) after rapid thermal annealing, and (c) after conventional thermal annealing.

Figure 4 shows AFM images of S1 and S2. The surface image is made by scanning over the sample surface in the X and Y directions. It is easy to see from the three-dimensional (3D) structure view that S1 has smaller grains on the surface and hence a larger surface area, as is shown in the SEM images.

Figure 5 shows the XRD analysis results obtained from S1 and S2, which are used to investigate the difference in the crystalline structures. The left side of Fig. 5 is a magnified image in the range of 22.0°–25.0°, and the strongest diffraction peak appears at $2\theta = 24.464°$, corresponding to the (200) plane, revealing a fine preferential growth of S1 in the [200] direction, whereas the peak of the (002) plane at $2\theta = 23.290°$ indicates that the growth of S2 was preferentially along the [002] direction.[27] Using Scherrer's formula and the full width at half maximum (FWHM) of the main peaks, it was estimated that the average particle sizes of S1 and S2 are 31.8980 nm and 51.4161 nm, respectively. A theoretical study showed that sensitivity for gas detection is significantly enhanced if the grain size is smaller than 50 nm,[28] and an XRD result confirmed this theoretical conclusion.

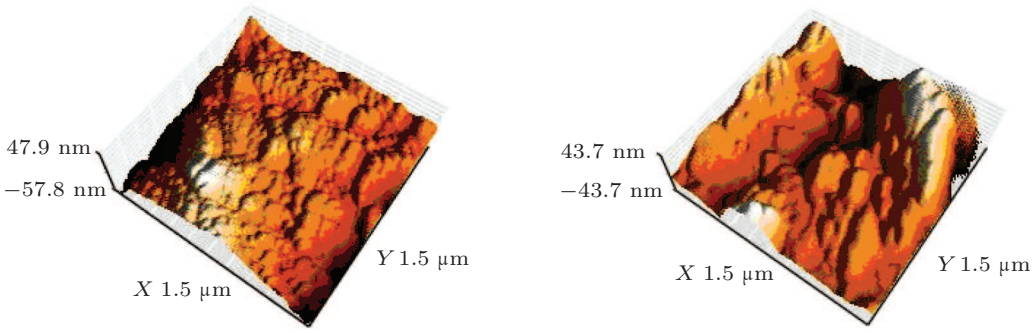


Fig. 4. (color online) Three-dimensional AFM images of S1 and S2 nanoparticle films after annealing.

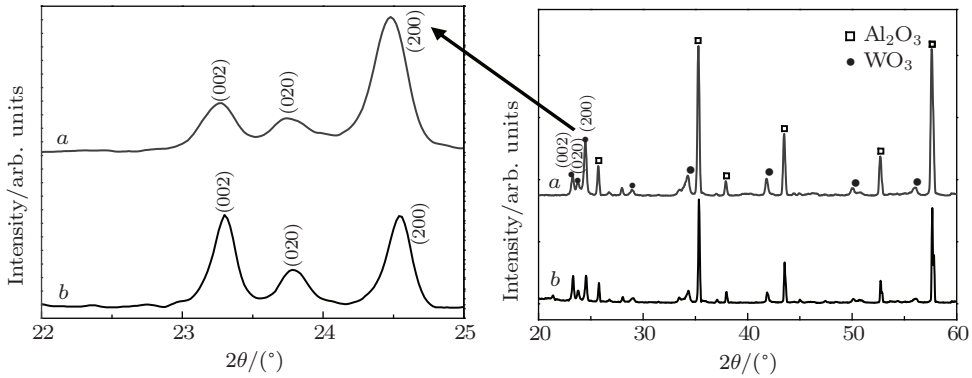


Fig. 5. XRD patterns of S1 (curve *a*) and S2 (curve *b*) after annealing.

3.2. NO_2-sensing properties

The NO_2-sensing measurement experiments were taken at RT under 40% relative humidity (RH). The resistance of the gas sensor was measured by the static gas-sensing testing system.

After stabilization of the sensor's signal in darkness, the LED lamp was switched on, supplying 397 nm light radiation with an intensity of 100 lx, which was controlled by the portable optometer. When the LED light was switched on, the resistance of the gas sensor began to decrease. After the stabilization of the resistance, NO_2 was injected into the test chamber with a micro-injector to obtain the desired concentration. S1 and S2 were measured in 1 ppm NO_2 gas, which was admitted and evacuated five times under constant light from the LED, and this shows the different performance under the same conditions. The continuous measurement result can be seen in Figs. 6(a)–6(b). After injecting NO_2, the resistance began to increase rapidly, then more slowly to stabilization. At this time, the testing chamber was opened, so as to displace the NO_2 with clear air. It can be seen that the resistance decreased. For S1, the resistance increases and decreases uniformly within a certain range and the sensitivity remains almost constant through five cycles; whereas S2 does not exhibit this characteristic, and its sensitivity declines (Fig. 7).

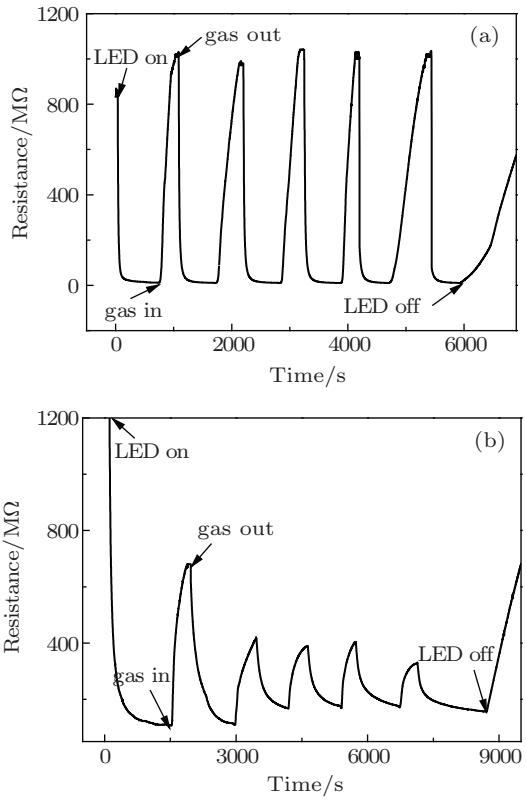


Fig. 6. Typical response-recovery curves of (a) S1 and (b) S2 to 1 ppm NO_2 gas. Five cyclic tests are shown, demonstrating the comparative stability of the gas sensors.

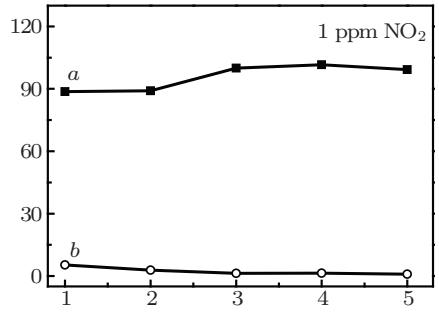


Fig. 7. The sensor sensitivity of (curve *a*) S1 and (curve *b*) S2 to 1 ppm NO_2, respectively.

In order to show the further superiority of S1, the sensor response of various NO_2 concentrations was measured. Figure 8 illustrates the dynamic response of S1 to NO_2 concentration in the range 0.1 ppm–5 ppm. All the measurements were taken under the LED light at RT.

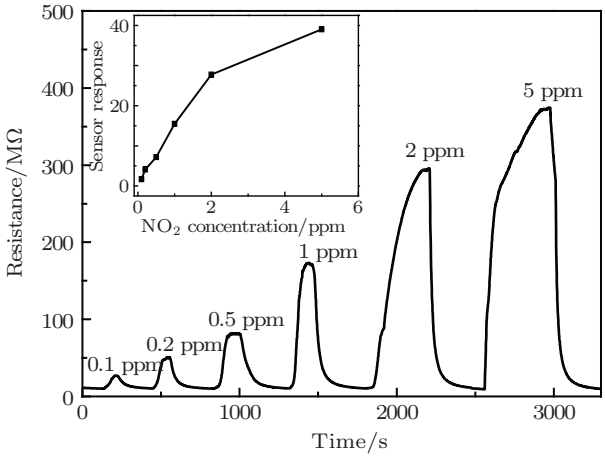


Fig. 8. The dynamic response curves of the S1 sample versus various concentrations of NO_2 at RT under LED radiation. Inset: the relationship between the gas sensor response values and the concentration of NO_2.

It can be concluded from the experiment that S1 has a sharply shorter recovery time (about 40 s) than S2 — the average recovery time of S2 is almost 10 times that of S1. But the response time of S1 is almost the same as that of S2.

The reasons for the different gas sensing properties are as follows. As is known, WO_3 is an n-type semiconductor. The electron concentration of WO_3 is determined mostly by the concentration of stoichiometric defects[29] such as oxygen vacancies. Molecules or atoms (O_2 or O) will be adsorbed on the surface in the form of O^-, O^{2-}, and O_2^-,[26] which extract electrons from the conduction band of the WO_3 thin film.[30] So electron-depleted space-charge layers are induced under the surface. When the n-type semiconductor is exposed to oxidizing gases such as NO_2, the gas molecules may be adsorbed onto the surface or react with the surface adsorbed species. As a result, the thickness of the electron-depleted layer and the height of the Schottky barrier will increase, leading to an increase in the sensor's resistance. A number of researchers[31] have indicated that the gas sensing properties of metal–oxide conductometric-type sensors can be greatly influenced by the surface interaction rate, grain size, grain network, and so on.[32] By comparing the average grain sizes of S1 and S2 (31.8980 nm and 51.4161 nm, respectively), it can be seen that the RTA treated film (S1, 31.8980 nm) has the smaller grain size. And from a theoretical study, it is known that the sensitivity for gas detection is significantly enhanced and the response to light is greater if the grain size is smaller than 50 nm.[28]

It seems that a small grain size enhances the photoactivation of WO_3 and makes gas sensors work at RT under LED radiation. When the LED light is switched on, the energy of the photons (397 nm, 3.1 eV) impinging on the surface is higher than the energy gap of the WO_3 (2.56 eV). So the change in conductance after illumination of the WO_3 thin film is believed to depend mainly on interband electronic transitions, considering that the energy of the photons is greater than the energy gap of WO_3. This is the reason why the conductance increases rapidly when the light is on and decreases after darkening.

When the LED light is on, conductance increases; it takes several minutes to establish a new equilibrium between the surface charge and the oxygen molecules of the gaseous phase. This low original resistance guarantees high sensitivity. When NO_2 is injected, the equilibrium is broken and the conductance decreases. After new equilibrium, the testing chamber is opened, admitting fresh air. The conductance increases with the help of LED radiation, the incident photons stimulating the creation of electron–hole couples inside the material. This is why the recovery time is much shorter.

3.3. Selectivity

Because WO_3[39] has a narrow gap ($\sim$ 2.56 eV), the WO_3 thin-film sensor can detect various gases, such as NO_2,[15,24,34–36] NH_3,[7,37,38] C_2H_5OH,[22,38] H_2, H_2S, and so

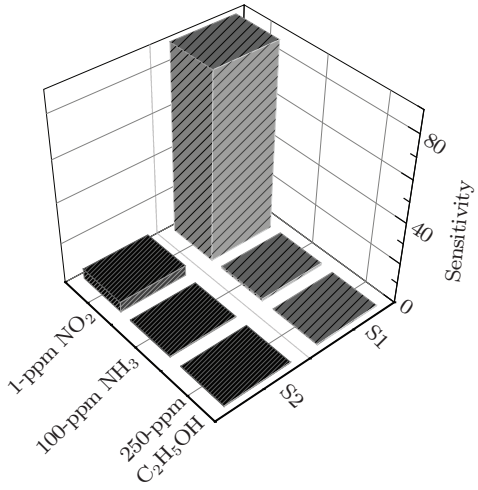


Fig. 9. Sensor responses of S1 and S2 to 1 ppm NO_2, 100 ppm NH_3, and 250 ppm C_2H_5OH under standard measuring conditions.

on. Figure 9 shows the response of sample S1 to 1 ppm NO_2, 100 ppm NH_3, and 250 ppm C_2H_5OH under standard measuring conditions with LED light. It can be seen from the figure that S1 has excellent selectivity for NO_2.

4. Conclusion

In this work, a thin-film WO_3 gas sensor was fabricated by applying rapid thermal annealing treatment to a WO_3 thin film deposited on an alumina substrate. SEM and AFM show that the surface has small particles and a structure with a high surface interaction rate. The XRD results confirm the formation of crystalline WO_3 with a grain size of about 31 nm. Compared with conventionally thermal-annealed WO_3 thin films, the RTA-treated WO_3 exhibits markedly high sensitivity to NO_2 and a short recovery time at RT under 100-lx LED radiation due to the high specific surface area and the small grain size. The results indicate the necessity of further research on the effects of RTA on metal–oxide thin-film gas sensors.

References

[1] Rava M, Verlato G and Bono R 2007 *Sci. Total Environ.* **384** 163
[2] Lin C Y, Fang Y Y, Lin C W, Tunney J J and Ho K C 2010 *Sens. Actuators B* **146** 28
[3] Chougule M A, Shashwati S and Patil V B 2012 *Sens. Actuators B* **38** 2685
[4] Kilinc N, Öztürk S, Arda L, Altindal A and Öztürk Z Z 2012 *J. Alloys Compd.* **536** 138
[5] Mohammadi M R, Fray D J 2007 *Acta Mater.* **55** 4455
[6] Moona H G, Janga H W, Kima J S, Parkb H H and Yoon S J 2011 *Sens. Actuators B* **153** 37
[7] Yuan H J, Chen Y Q, Yu F, Peng Y H, He X W, Zhao D and Tang D S 2011 *Chin. Phys. B* **20** 036103
[8] Li S, Li F L, Zhou S M, Wang P, Cheng K and Du Z L 2009 *Chin. Phys. B* **18** 3985
[9] Liu L, Zhang T, Li S C, Wang L Y, Fan H T and Li W 2009 *Chin. Phys. Lett.* **26** 100702
[10] Qiao J P, Zhu Z P, Yan X Y and Qin J M 2011 *Chin. Phys. Lett.* **29** 020701
[11] Yue X J, Hong T S, Xu X and Li Z 2011 *Chin. Phys. Lett.* **28** 090701
[12] Xu L, Wang R, Xiao Q, Zhang D and Liu Y 2011 *Chin. Phys. Lett.* **28** 070702
[13] Liu L, Kou L Y, Zhong Z C, Wang L Y, Liu L F and Li W 2010 *Chin. Phys. Lett.* **27** 050701
[14] Sun F Y 2010 "Study and Preparation of Low Power Porous Silicon Based Tungsten Oxide Film Gas Sensors" Ph. D. dissertation, Tianjin University (in Chinese)
[15] Chen H Q, Hu M, Zeng J and Wang W D 2012 *Chin. Phys. B* **21** 058201
[16] Haridas D, Chowdhuri A, Sreenivasa K and Guptaa V 2011 *Sens. Actuators B* **153** 152
[17] Deng L B, Ding X H, Zeng D W, Tian S Q, Li H Y and Xie C S 2012 *Sens. Actuators B* **163** 260
[18] Chen S H, Chen J, Deng S Z and Xu N S 2010 *Chin. Phys. B* **19** 037803
[19] Polleux J, Gurlo A, Barsan N, Weimar U, Antonietti M and Niederberger M 2006 *Angew. Chem. Int. Ed.* **45** 261
[20] Liu Z, Yamazaki T, Shen Y, Meng D, Kikuta T, Nakatani N and Kawabata T 2008 *J. Phys. Chem. C* **112** 1391
[21] Pokhrel S, Simion C E, Teodorescu V S, Barsan N and Weimar U 2009 *Adv. Funct. Mater.* **19** 1767
[22] Labidi A, Gillet E, Delamare R, Maaref M and Aguir K 2006 *Sens. Actuators B* **120** 338
[23] Solis J L, Saukko S, Kish L, Granqvist C G and Lantto V 2001 *Thin Solid Films* **391** 255
[24] Penza M, Martucci C and Cassano G 1998 *Sens. Actuators B* **50** 52
[25] Qin Y X, Shen W J, Li X and Hu M 2011 *Sens. Actuators B* **155** 646
[26] Qin Y X, Hu M and Zhang J 2010 *Sens. Actuators B* **150** 339
[27] Hu M, Wang W D, Zeng P, Zeng J and Qin Y X 2012 *Chin. Phys. B* **21** 023101
[28] Wang X, Yee S S and Carey W P 1995 *Sens. Actuators B* **25** 454
[29] Wang Y D, Chen Z X, Li Y F, Zhou Z L and Wu X H 2001 *Solid State Electron.* **45** 639
[30] Guerin J, Aguir K and Bendahan M 2006 *Sens. Actuators B* **119** 327
[31] Zeng J, Hu M, Wang W D, Chen H Q and Qin Y X 2012 *Sens. Actuators B* **161** 447
[32] Korotcenkov G 2008 *Mater. Sci. Eng. R* **61** 1
[33] Hu M, Wang W D, Zeng J and Qin Y X 2011 *Chin. Phys. B* **20** 102101
[34] Ma H L, Fan D W and Niu X S 2010 *Chin. Phys. B* **19** 076102
[35] Qin Y X, Wang F, Shen W J and Hu M 2010 *Acta Phys. Sin.* **61** 057301 (in Chinese)
[36] Qin Y X, Li X, Wang F and Hu M 2011 *J. Alloys Compd.* **509** 8401
[37] Hu M, Zhang J, Wang W D and Qin Y X 2011 *Chin. Phys. B* **20** 082101
[38] Sun F Y, Hu M, Sun P, Zhang J and Liu B 2010 *J. Nanosci. Nanotechnol.* **10** 7739
[39] Wang C, Wang F F, Fu X Q, Zhang E D and Xu Z 2011 *Chin. Phys. B* **20** 050701